Scientific Research Publishing

Smart Grid and Renewable Energy, 2023, 14, 85-106
https://www.scirp.org/journal/sgre
ISSN Online: 2151-4844
ISSN Print: 2151-481X

An Energy Production System Powered by Solar Heat with Biogas Dry Reforming Reactor and Solid Oxide Fuel Cell

Akira Nishimura[1], Ryotaro Sato[1], Eric Hu[2]

[1]Division of Mechanical Engineering, Graduate School of Engineering, Mie University, Tsu, Japan
[2]School of Electrical Mechanical Engineering, The University of Adelaide, Adelaide, Australia
Email: nisimura@mach.mie-u.ac.jp

How to cite this paper: Nishimura, A., Sato, R. and Hu, E. (2023) An Energy Production System Powered by Solar Heat with Biogas Dry Reforming Reactor and Solid Oxide Fuel Cell. *Smart Grid and Renewable Energy*, **14**, 85-106.
https://doi.org/10.4236/sgre.2023.145006

Received: April 25, 2023
Accepted: May 28, 2023
Published: May 31, 2023

Abstract

In this paper, an energy system consisting of solar collector, biogas dry reforming reactor and solid oxide fuel cell (SOFC) has been proposed. The heat produced from the concentrating solar collector is used to drive a biogas dry reforming reactor in order to produce H_2 as a fuel for SOFC, in such as system. The aim of this study is to clarify the impact of climate data on the performance of solar collector with various sizes/designs. The temperature of heat transfer fluid produced by the solar collector is calculated by adopting the climate data for Nagoya city in Japan in 2021. The amount of H_2 produced from the biogas dry reforming reactor and the power generated by SOFC were simulated. The results show the temperature of heat transfer fluid (T_{fb}) and T_{fb} ratio (a) based on the length of absorber (dx) = 1 m have a peak near the noon following the trend of solar intensity (I). Results also revealed that a increases with increase in dx. It is found that the differences of T_{fb} and a between dx = 2 m and dx = 3 m are larger than those between dx = 1 m and dx = 2 m. It is revealed that T_{fb} and a are higher in spring and summer. dx = 4 m is the optimum length of solar absorber. The amount of H_2 produced from the biogas dry reforming reactor as well as the power generated by SOFC is the highest in August, resulting that it is prefer to produce H_2 and to generate SOFC in summer.

Keywords

Solar Collector, Fluid Temperature, Climate Data, Biogas Dry Reforming, H_2 Production, SOFC

1. Introduction

Global warming has been a serious problem in the world. Renewable energy is

one of promising procedure to solve the global warming problem. According to Energy White Paper 2022 in Japan [1], the ratio of renewable energy to the whole energy consumption in the world is 5.7% in 2020. To realize a net zero emission society, it is suggested that the supply of renewable energy should be 7919 million oil equivalent tons in 2050, while the whole energy supply is 12,967 million oil equivalent ton [1]. As the other procedure to solve the global warming problem, a renewable H_2 is a candidate. H_2O is emitted only after utilization of H_2O as a fuel for fuel cell. There are several techniques to produce H_2 from fossil fuels such as natural gas, coal and oil. However, they are needed to combine the carbon capture storage (CCS) or usage (CCU) technology for realization of a net zero emission society.

This study focuses on a biogas dry reforming to produce H_2. Biogas is a gaseous fuel consisting of CH_4 (55 - 75 vol%) and CO_2 (25 - 45 vol%) [2], mainly produced from fermentation by the action of anaerobic microorganisms on raw materials such as, garbage, livestock excretion, and sewage sludge. Additionally, the conversion of biogas to H_2 can be said as a carbon neutral since the CO_2, which is a by-product in the biogas production process, can be absorbed by plants. It is reported from the International Energy Agency (IEA) [3] that the biogas has been produced 62.3 billion·m^3 globally with an equivalent energy of 1.43 EJ in 2019. The amount of produced biogas in 2019 has been five times as large as that in 2000. Consequently, it is thought that the biogas is a promising energy source. Generally speaking, the biogas is used as a fuel for gas engine or micro gas turbine [4]. Since a biogas contains CO_2 of approximately 40 vol%, the efficiency of power generation decreases due to smaller heating value compared to natural gas. This study proposes the H_2 production from biogas dry reforming to utilize as a fuel for solid oxide fuel cell (SOFC) system. SOFC can also use CO which is a by-product from biogas dry reforming as a fuel, resulting in the effective energy production system.

Since the biogas dry reforming is an endothermic reaction, this study proposes the combination system with a solar collector. In the previous studies by the authors [5] [6], the biogas dry reforming has been conducted by the heat input using the electric heater. Then, CO_2 is emitted due to usage of the electricity generated by Japanese electric power company which uses a fossil fuel actually now. Therefore, the authors hit on the new system consisting of solar collector, biogas dry reforming reactor and SOFC. There is no previous report on the concept of this type.

According to the literature survey by the authors, a parabolic trough collector is the most established solar concentration technology worldwide [7]. The temperature of heat transfer fluid can be attained approximately 723 K by a parabolic trough collector [7] [8] [9]. The impact of concentration ratio on the relationship between the temperature of heat transfer fluid and energy efficiency was investigated [8]. The concentration ratio was changed from 10 to 30. There is the optimum concentration ratio to obtain the higher temperature of heat transfer fluid, which is the concentration ratio of 20. The effect of configuration of para-

bolic trough collector, e.g. solar incidence angle [9] on the collector efficiency and the optimal loss was investigated. When the mass flow rate of heat transfer fluid increases, the heat loss decreases due to promotion of convective heat transfer between the tube wall and the heat transfer fluid. There are several reports on the heat transfer model for investigation of parabolic trough collector [8] [9] [10] [11]. The heat transfer model considers a conduction, a convection and a radiation heat transfer. The double pipes structure model considering heat loss to the atmosphere can estimate the temperature of heat transfer fluid changing the solar intensity, the mass flow rate of fluid, the diameter and length of glass tube [10]. Though the previous studies developed the heat transfer model, there is no study investigating the impact of climate data on the performance of solar collector changing the shape of solar collector. In addition, there is no study to estimate the amount of H_2 produced from the biogas dry reforming reactor when assuming to use the heat obtained from the solar collector for the biogas dry reforming. Moreover, there is no study to estimate the power generated by SOFC consisting of solar collector and biogas dry reforming reactor.

The aim of this study is to clarify the impact of climate data on the performance of solar collector changing the shape of solar collector. This study refers the developed heat transfer model investigating the parabolic trough collector [10]. The temperature of heat transfer fluid is calculated by adopting the climate data for Nagoya city in Japan in 2021 [12]. The diameter and the length of heat absorber are changed for this analysis. In addition, this study also aims to estimate the amount of H_2 produced from the biogas dry reforming reactor when assuming to use the heat obtained from the solar collector for the conduction of biogas dry reforming. In this study, the specific characteristics of biogas dry reforming reactor developed by the authors [5] [6] are adopted to estimate the amount of produced H_2. Moreover, this study also aims to estimate the power generated by SOFC consisting of solar collector and biogas dry reforming reactor. The power generation efficiency of commercial SOFC is adopted to estimate the power generated by SOFC in this study.

2. Analysis Procedure

2.1. Heat Transfer Model for Solar Collector

Figure 1 illustrates the schematic diagram for heat transfer model of parabolic trough collector. The heat transfer mechanism in this model is explained in the caption of **Figure 1**. **Figure 2** shows the thermal resistance distance diagram for the heat transfer process in this model. Each thermal resistance is explained in the caption of **Figure 2**.

This study assumes that the surrounding surface temperature is equal to the ambient air temperature. The model equation for a single glass cover can be explained as follow [10]:

$$I\alpha\tau D\pi dx = \frac{T_{to} - T_{fb}}{R_1} + \frac{T_{to} - T_s}{\left(R_5^{-1} + R_6^{-1}\right)^{-1}} \quad (1)$$

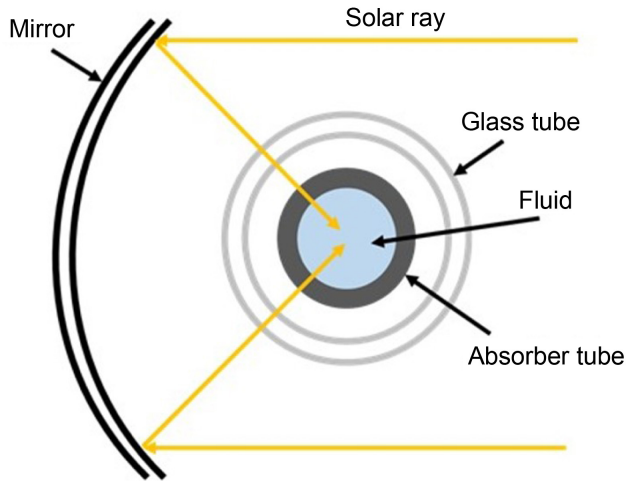

Figure 1. Schematic diagram for heat transfer model of parabolic trough solar collector (A solar radiation is mainly absorbed at the outlet surface of the absorber tube as a heat [10]. Some parts of the absorbed heat transports to the working/heat transfer fluid by conduction through tube wall and convection from the inner surface of the tube to the fluid. Other parts of the heat transfers as a loss by radiation to the inner surface of the glass through the vacuum space and then by conduction from the inner surface of the glass to the outer surface of the glass. The heat transferred to ambient from the outlet surface of the glass by two mechanisms, *i.e.* the convection to the surrounding air and the radiation to the surrounding surfaces, e.g. buildings and sky).

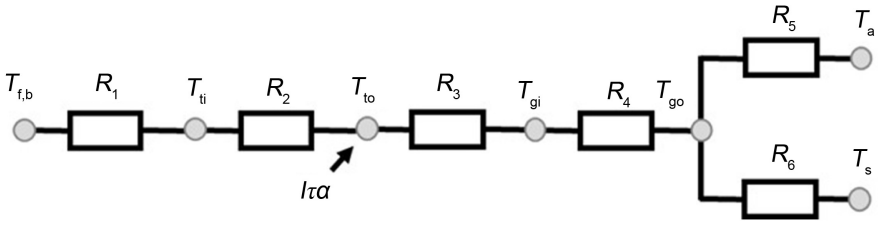

Figure 2. Thermal resistances diagram of the heat transfer model in this study (R_1: thermal resistance by thermal convection from the heat transfer fluid to the absorber [K/W], R_2: thermal resistance by thermal conduction through the absorber [K/W], R_3: thermal resistance by radiation through vacuum [K/W], R_4: thermal resistance by thermal conduction through the glass tube [K/W], R_5: thermal resistance by thermal convection to the ambient air [K/W] and R_6: thermal resistance by radiation to the surrounding surfaces (buildings and sky)).

$$mc\frac{dT_{fb}}{dx} = mc\frac{T_{fb,out} - T_{fb,in}}{dx} = \frac{T_{to} - T_{fb}}{R_1} \tag{2}$$

$$\frac{T_{to} - T_{gi}}{R_3} = \frac{T_{to} - T_s}{R_3 + \left(R_5^{-1} + R_6^{-1}\right)^{-1}} \tag{3}$$

where, I means a solar intensity [W/m^2], α means an absorptivity of absorber tube [-], τ means a transmissivity of glass tube [-], D means a diameter of absorber [m], dx means a length of absorber [m], m means a mass flow rate of heat transfer fluid which is assumed to be a biogas [kg/s], c is a specific heat of heat transfer fluid [J/(kg·K)], T_{fb} means a temperature of heat transfer fluid [K], $T_{fb,out}$

means a temperature of heat transfer fluid at outlet [K] and $T_{fb,in}$ means a temperature of heat transfer fluid at inlet [K]. Each thermal resistance can be defined as follows:

$$R_1 = \frac{1}{2\pi r_{ti} h} \tag{4}$$

$$R_2 = \frac{1}{2\pi k_t} \ln \frac{r_{to}}{r_{ti}} \tag{5}$$

$$R_3 = \frac{1}{2\pi\sigma r_{to}} \left[\frac{1}{\varepsilon_t} + \frac{1-\varepsilon_g}{\varepsilon_g} \left(\frac{r_{to}}{t_{gi}} \right) \right] \left[\left(T_{to}^2 + T_{gi}^2 \right) \left(T_{to} + T_{gi} \right) \right]^{-1} \tag{6}$$

$$R_4 = \frac{1}{2\pi k_g} \ln \frac{r_{go}}{r_{gi}} \tag{7}$$

$$R_5 = \frac{1}{2\pi r_{go} h_o} \tag{8}$$

$$R_6 = \frac{1}{\varepsilon_g \sigma 2\pi r_{go} \left(T_{go} + T_s \right) \left(T_{go}^2 + T_s^2 \right)} \tag{9}$$

where, r_{ti} means an inside radius of absorber [m], r_{to} means an outside radius of absorber [m], r_{gi} means an inside radius of glass tube [m], r_{go} means an outside radius of glass tube [m], σ means Stefan-Boltzmann constant [W/(m^2·K^4)], h means the heat transfer coefficient between heat transfer fluid and inside surface of absorber [W/(m^2·K)], h_o means the heat transfer coefficient from outside surface of glass tube to atmosphere [W/(m^2·K)], k_t means a thermal conductivity of absorber [W/(m·K)], k_g means a thermal conductivity of glass tube [W/(m·K)], ε_t means an emissivity of absorber [-], ε_g means an emissivity of glass tube [-], T_{to} means a temperature of outside surface of absorber [K], T_{gi} means a temperature of inside surface of glass tube [K], T_{go} means a temperature of outside surface of glass tube [K], T_s means a temperature of surroundings surface [K], and T_a means a temperature of surrounding air [K].

2.2. Estimation of Heat Transfer Coefficient

In this study, the heat transfer coefficient for the turbulent flow in a tube is followed by Dittus-Boelter correlations [13]:

$$\mathrm{Nu} = 0.023\,\mathrm{Re}^{0.8}\,\mathrm{Pr}^{1/3} \tag{10}$$

$$\mathrm{Nu} = \frac{hD}{k_a} \tag{11}$$

$$\mathrm{Re} = \frac{\rho_a u_a D}{\mu_a} \tag{12}$$

$$\mathrm{Pr} = \frac{C_{p,a}\mu_a}{k_a} \tag{13}$$

$$h_o = 0.0191 + 0.006608 u_a \tag{14}$$

where, $C_{p,a}$ means a specific heat of surrounding air [J/(kg·K)], μ_a means a vis-

cosity [Pa·s], k_a means a thermal conductivity of surrounding air [W/(m·K)], u_a means a velocity of surrounding air [m/s] and ρ_a means a density of surrounding air [m/s].

2.3. Calculation Procedure

According to Equations (1) and (2), the following equation can be obtained:

$$T_{fb,out} = \frac{dx}{mc}\left\{I\alpha\tau D\pi dx - \frac{\left(T_{to} - T_s\right)\left(R_5 + R_6\right)}{R_3\left(R_5 + R_6\right) + R_5R_6}\right\} + T_{fb,in} \tag{15}$$

Moreover, R_3 is obtained according to Equation (3) as follows:

$$R_3 = \frac{\left(T_{to} - T_{gi}\right)R_5R_6}{\left(R_5 + R_6\right)\left(-T_s + T_{gi}\right)} \tag{16}$$

From Equations (6) and (16), T_{to} can be calculated as follows:

$$T_{to} = \left[\frac{\left(R_5 + R_6\right)\left(-T_s + T_g\right)}{2\pi\sigma r_{to}R_5R_6} \times \frac{\left\{r_{gi} + r_{to}\left(1 - \varepsilon_g\right)\right\}}{\varepsilon_t r_{gi}} + T_{gi}^4\right]^{\frac{1}{4}} \tag{17}$$

In this study, T_{fb} is estimated by averaging $T_{fb,\,in}$ and $T_{fb,\,out}$ as follows:

$$T_{fb} = \frac{T_{fb,out} + T_{fb,in}}{2} \tag{18}$$

This study calculates T_{fb} changing D and dx according to the above equations when inputting the climate data, *i.e.* I, u_a and T_a in Nagoya city in Japan in 2021 [12]. The heat transfer fluid used in this study is CH_4 and CO_2 mixture with the molar ratio of CH_4:CO_2 is 1.5:1. The molar ratio of CH_4:CO_2 is 1.5:1 which simulates the biogas. In this study, the following assumptions were made as follows:

1) The mass flow rate of the heat transfer fluid (m) is 0.05 kg/s.

2) The distance between absorber and glass tube is 1/10 D.

3) $T_{fb,\,in}$ is 283 K.

4) T_s equals to T_a.

5) The thickness of absorber and glass tube is 0.005 m and 0.010 m, respectively.

6) R_2 and R_4 are ignored since they are very small compared to the other thermal resistances [10].

7) T_{ti} equals to T_{to}.

8) T_{gi} equals to T_{go}, which is 373 K.

The values of physical properties used in this study are listed in **Table 1**.

Figure 3 illustrates the system consisting of solar collector, biogas dry reforming reactor and SOFC proposed by this study. The flow is explained in the caption of **Figure 3**.

To estimate the amount of H_2 produced from the biogas dry reforming reactor, this study follows the reaction scheme of biogas dry reforming as follows:

Table 1. The physical properties used in this study [10] [14].

Property	Value	Information
α [-]	0.94	[10]
τ [-]	0.94	[10]
ε_t [-]	0.9	[10]
c [J/(kg·K)]	1335	for CH_4:CO = 1.5:1 [14]
σ [W/(m^2·K^4)]	5.67×10^{-8}	Stefan-Boltzmann coefficient
ε_g [-]	0.94	Glass smooth surface [14]
k_a [W/(m·K)]	0.0257	Surrounding air [14]
ρ_a [kg/m^3]	1.166	Surrounding air [14]
μ_a [Pa·s]	1.82×10^{-5}	Surrounding air [14]
$C_{p,a}$ [J/(kg·K)]	1006	Surrounding air [14]
k_t [W/(m·K)]	16	Stainless steel [14]
k_g [W/(m·K)]	1.3	Quartz glass [14]

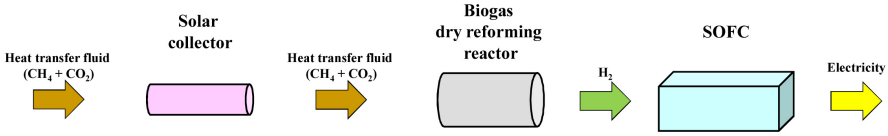

Figure 3. System consisting of solar collector, biogas dry reforming reactor and SOFC proposed by this study (Heat transfer fluid consisting of CH_4 and CO_2 flows into solar collector. After heated by solar collector, the heat transfer fluid flows into biogas fry reforming reactor. After the reaction by biogas dry reforming, H_2 is produced. The produced H_2 is supplied into SOFC as a fuel, resulting that the electricity is generated).

$$CH_4 + CO_2 \rightarrow 2H_2 + 2CO \tag{19}$$

In this study, the molar flow rate of CO_2 and CH_4 is 1.67×10^{-2} mol/s and 2.51×10^{-2} mol/s, respectively, which presents the molar ratio of CH_4:CO_2 of 1.5:1 and m of 0.05 kg/s. According to Equation (19) and these molar flow rates, the molar flow rate of produced H_2 can be calculated to be 3.34×10^{-2} mol/s. According to the authors' previous experimental studies changing the reaction temperature, which corresponds to T_{fb} in this study, from 673 K to 873 K [5] [6], the performance of biogas dry reforming is the best at 873 K. Consequently, this study assumes H_2 can be produced by biogas dry reforming at T_{fb} over 873 K. The conversion ratio of H_2 is changed by 1%, 10% and 100%. According to the authors' previous experimental studies [5] [6], the highest conversion ratio of H_2 was approximately 10%. This study adopts the conversion ratio of H_2 of 10% following the experimental result and also adopts that of 1% and 100% as the assumed minimum and maximum performance case, respectively.

To estimate the power generated by SOFC, this study considers the lower heating value of H_2 (=10.79 MJ/m^{3}N) and the power generation efficiency of commercial SOFC of 55% [15]. When the conversion ratio of H_2 is 100%, the

power generated by SOFC can be calculated as follows:

$$\left(3.34\times10^{-2}\left[\mathrm{mol/s}\right]\right)\times\left(22.4\left[\mathrm{L/mol}\right]\right)\div\left(1000\left[\mathrm{L/m^3}\right]\right)\times0.55\times\left(10.79\left[\mathrm{MJ/m^3\cdot N}\right]\right)=4.44\left[\mathrm{kW}\right] \tag{20}$$

The amount of produced H_2 and the power generated by SOFC which are estimated by this study under several conditions are shown and discussed in the next section.

3. Results and Discussion

3.1. Calculation on Temperature of Heat Transfer Fluid

At first, the climate data, *i.e.* I, u_a and T_a in Nagoya city in Japan in 2021 [12] which are used for the calculation of T_{fb} are shown. In Tables 2-5, the data in January, April, July and October are listed as a representative data for Winter, Spring, Summer and Autumn, respectively. The monthly mean values are listed in these tables.

Figures 4-7 show T_{fb} with time changing D and dx among different months. In Figures 4-7, the data in January, April, July and October are listed as a representative data for Winter, Spring, Summer and Autumn, respectively. The monthly mean value is shown in these figures. In addition, Figures 8-11 show the T_{fb} ratio (a) based on dx = 1 m with time changing D and dx among different months. a is defined as follows:

$$a=\frac{T_{fb}\left(dx=2\text{ m}\sim5\text{ m}\right)}{T_{fb}\left(dx=1\text{ m}\right)} \tag{21}$$

Table 2. Climate data of I, u_a and T_a in Nagoya city in January.

Time	I [MJ/m^2]	u_a [m/s]	T_a [K]
6:00	0	2.1	275.4
7:00	0	2.2	275.3
8:00	43.8	2.2	275.8
9:00	166.6	2.4	277.0
10:00	295.3	2.7	278.4
11:00	379.0	3.4	279.5
12:00	398.4	3.6	280.3
13:00	422.5	3.8	280.6
14:00	369.0	3.9	281.0
15:00	288.3	3.9	280.9
16:00	168.7	4.0	280.4
17:00	46.8	3.5	279.7
18:00	0.6	3.2	279.0
19:00	0	2.8	278.5

Table 3. Climate data of I, u_a and T_a in Nagoya city in April.

Time	I [MJ/m^2]	u_a [m/s]	T_a [K]
6:00	15.8	2.7	284.6
7:00	114.3	2.8	285.5
8:00	274.9	3.0	286.9
9:00	428.7	3.2	288.3
10:00	562.8	3.4	289.7
11:00	639.5	3.7	290.7
12:00	690.1	3.6	291.7
13:00	669.3	4.2	292.3
14:00	592.2	4.7	292.3
15:00	505.8	4.8	292.1
16:00	376.9	5.0	291.6
17:00	231.3	5.0	290.8
18:00	83.3	4.9	289.8
19:00	4.8	4.5	288.9

Table 4. Climate data of I, u_a and T_a in Nagoya city in July.

Time	I [MJ/m^2]	u_a [m/s]	T_a [K]
6:00	33.6	1.4	298.2
7:00	133.8	1.6	298.9
8:00	279.7	1.8	299.9
9:00	408.4	1.9	300.9
10:00	530.7	2.2	301.9
11:00	623.8	2.7	302.9
12:00	603.6	3.0	303.2
13:00	581.2	3.2	303.6
14:00	526.6	3.6	303.5
15:00	485.2	4.0	303.1
16:00	353.5	3.8	302.8
17:00	223.7	3.9	301.9
18:00	133.0	3.7	301.3
19:00	37.4	3.3	300.7

In Figures 8-11, the data in January, April, July and October are listed as a representative data for Winter, Spring, Summer and Autumn, respectively. Additionally, in Figures 8-11, the gray area indicates that there is no shining.

Table 5. Climate data of I, u_a and T_a in Nagoya city in October.

Time	I [MJ/m^2]	u_a [m/s]	T_a [K]
6:00	0.4	2.1	289.6
7:00	45.1	2.2	290.1
8:00	178.1	2.6	291.3
9:00	324.5	2.7	292.8
10:00	470.5	3.0	294.2
11:00	543.5	3.0	295.4
12:00	555.4	3.3	296.1
13:00	503.3	3.5	296.5
14:00	421.4	3.6	296.7
15:00	346.1	3.9	296.6
16:00	219.0	3.8	296.0
17:00	85.8	3.7	295.1
18:00	5.3	3.6	294.2
19:00	0	3.1	293.4

It is seen from Figures 4-11 that T_{fb} and a have a peak near the noon. This is followed by the trend of Ias shown in Tables 2-5. In addition, it is found from Figures 4-7 that T_{fb} for $dx = 1$ m keeps low value irrespective of D. According to Equation (19), it is known that dx has more impact compared to D from the view point of digit. It is seen from Figures 8-11 that a increases with increase in dx. Since the surface area for absorbing solar heat increases, the amount of absorbed heat increases. Moreover, it is known from Figures 4-11 that the differences of T_{fb} and a between $dx = 2$ m and $dx = 3$ m are larger than those between $dx = 1$ m and $dx = 2$ m. This is because Equation (15) has the term of dx^2.

Investigating the effect of the season on T_{fb} and a, the highest T_{fb} is obtained for April, which is 2400 K. The 2nd highest T_{fb} is obtained for July. Comparing four seasons, T_{fb} and a are higher in spring and summer, while they are lower in autumn and winter. These results follow the data of I. In addition, it is revealed from Figures 4-7 that T_{fb} is over 873 K for $D = 1.0$, 1.5 m and $dx = 4$, 5 m except for winter. However, it is known that T_{fb} is too high for $D = 1.5$ m and $dx = 5$ m, e.g. $T_{fb} = 2199$ K as shown in Figure 6. Since it is the excess heated temperature for the material of solar absorber, it can claim that $dx = 4$ m is the optimum length of solar absorber.

3.2. Estimation of the Amount of H_2 Produced from Biogas Dry Reforming Reactor

To estimate the amount of H_2 produced from the biogas dry reforming reactor, Table 6 lists the time when T_{fb} is over 873 K. The time when T_{fb} is over 873 K is

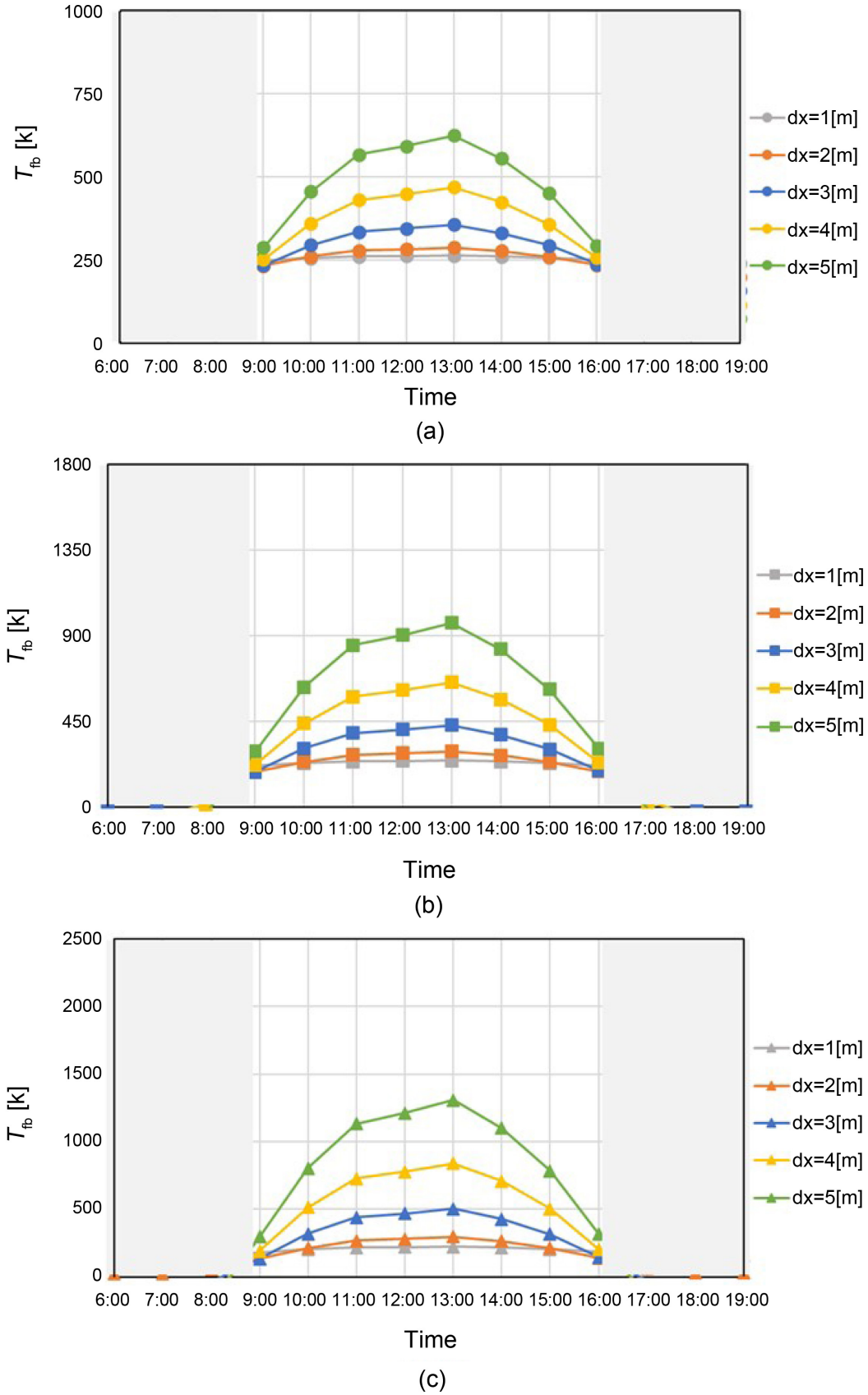

Figure 4. T_{fb} with time changing D in January ((a): $D = 0.5$ [m], (b): $D = 1.0$ [m], (c): $D = 1.5$ [m]).

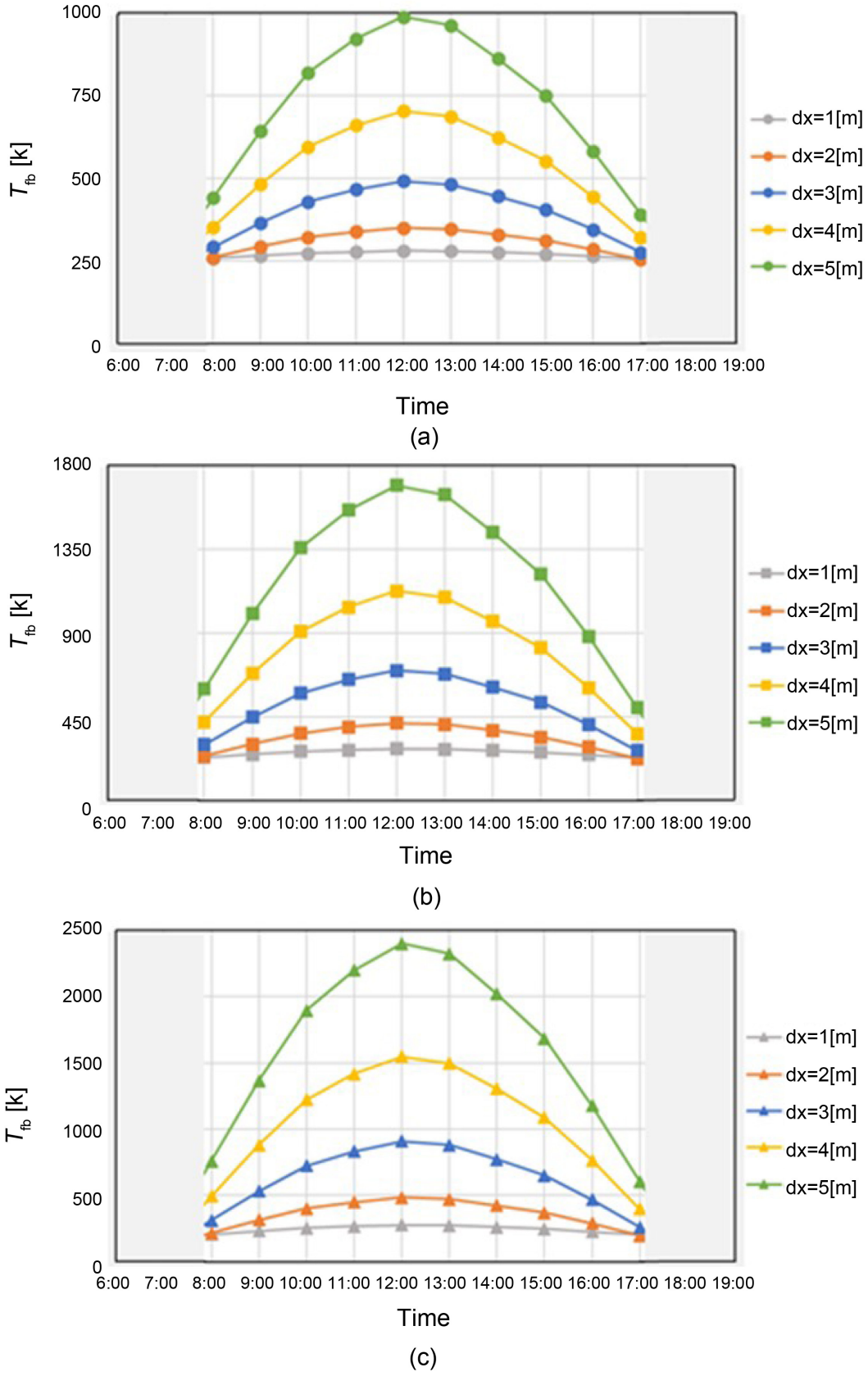

Figure 5. T_{fb} with time changing D in April ((a): $D = 0.5$ [m], (b): $D = 1.0$ [m], (c): $D = 1.5$ [m]).

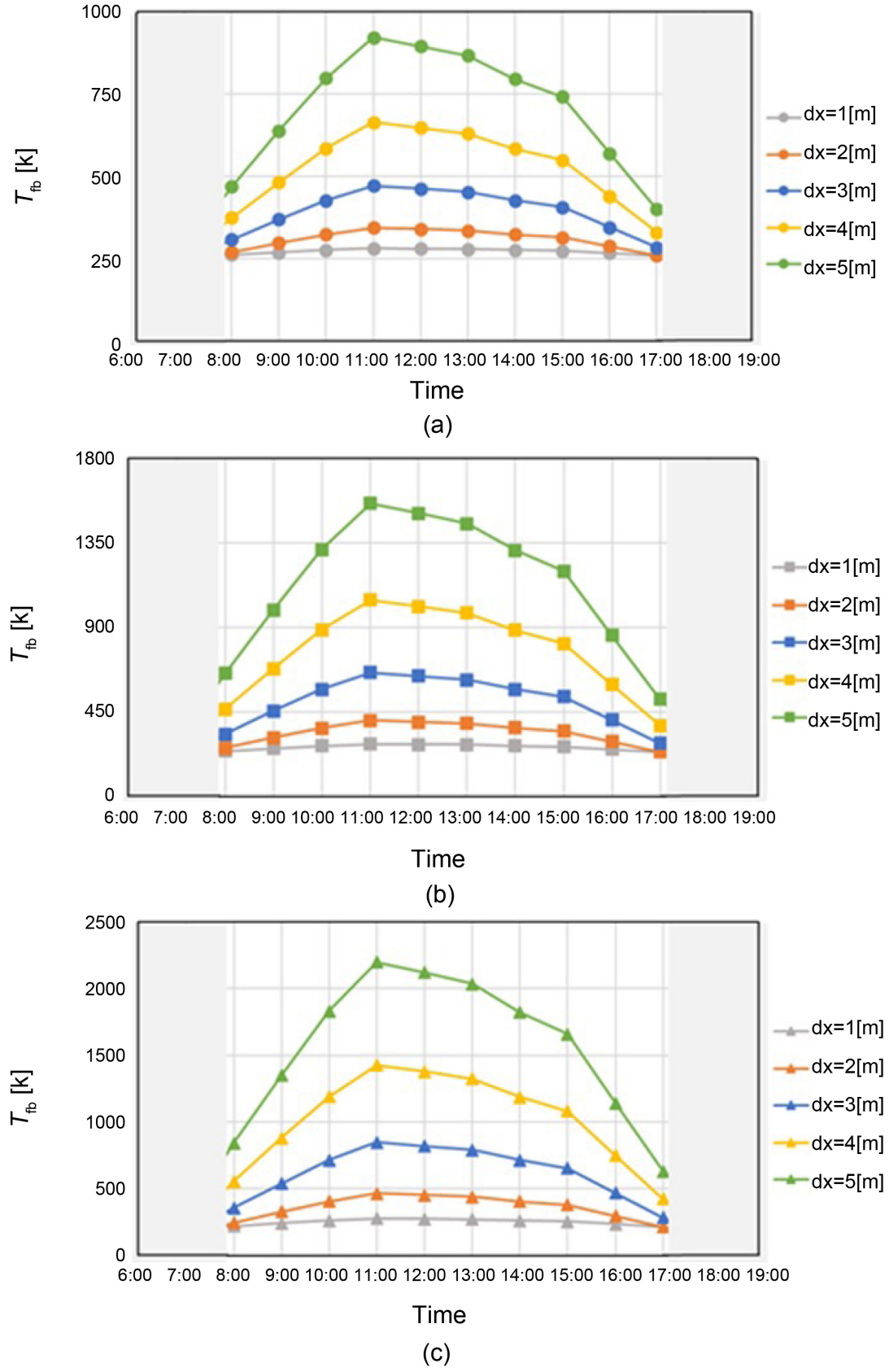

Figure 6. T_{fb} with time changing D in July ((a): $D = 0.5$ [m], (b): $D = 1.0$ [m], (c): $D = 1.5$ [m]).

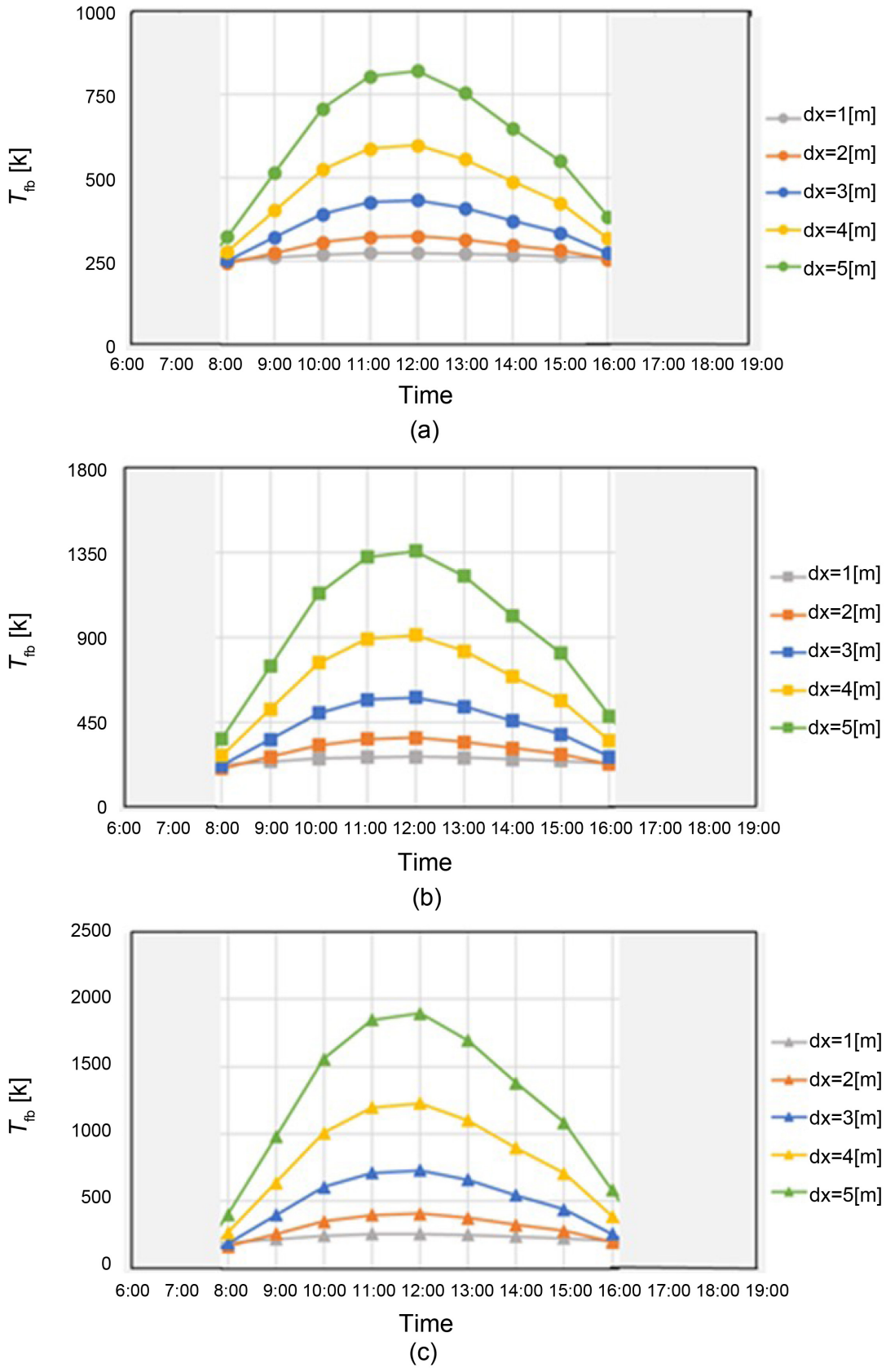

Figure 7. T_{fb} with time changing D in October ((a): $D = 0.5$ [m], (b): $D = 1.0$ [m], (c): $D = 1.5$ [m]).

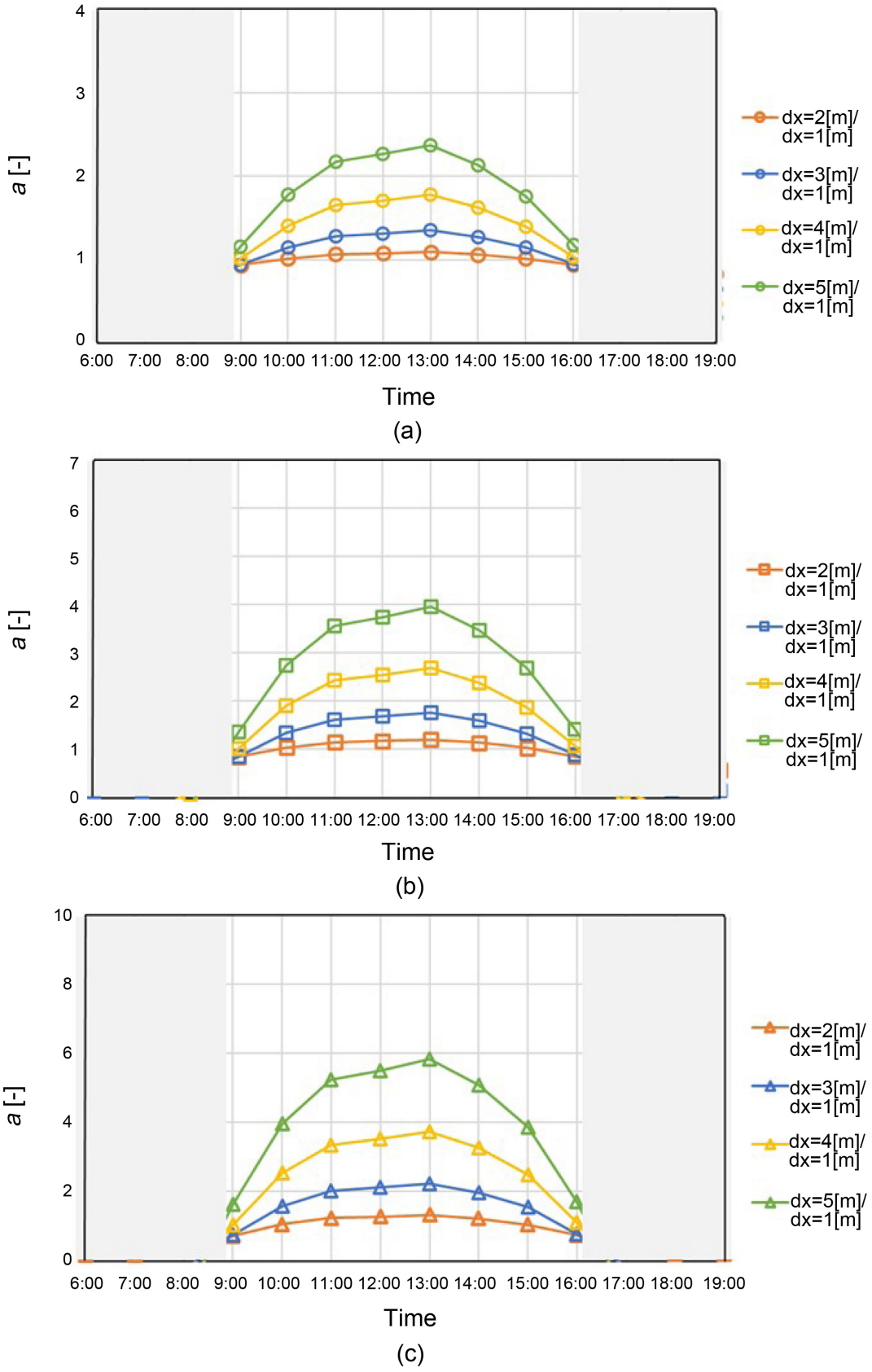

Figure 8. *a* with time changing *D* in January ((a): *D* = 0.5 [m], (b): *D* = 1.0 [m], (c): *D* = 1.5 [m]).

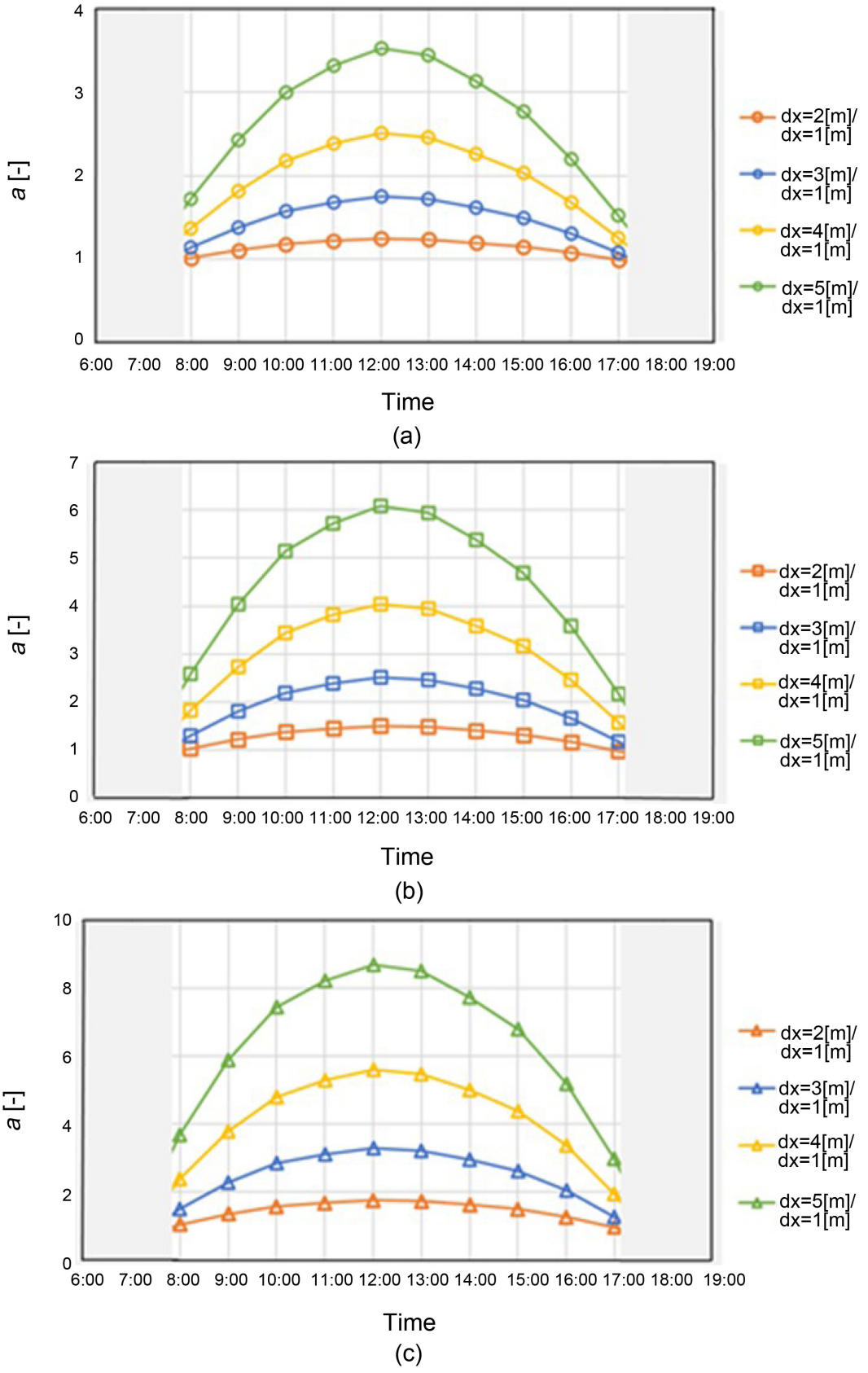

Figure 9. *a* with time changing D in April ((a): $D = 0.5$ [m], (b): $D = 1.0$ [m], (c): $D = 1.5$ [m]).

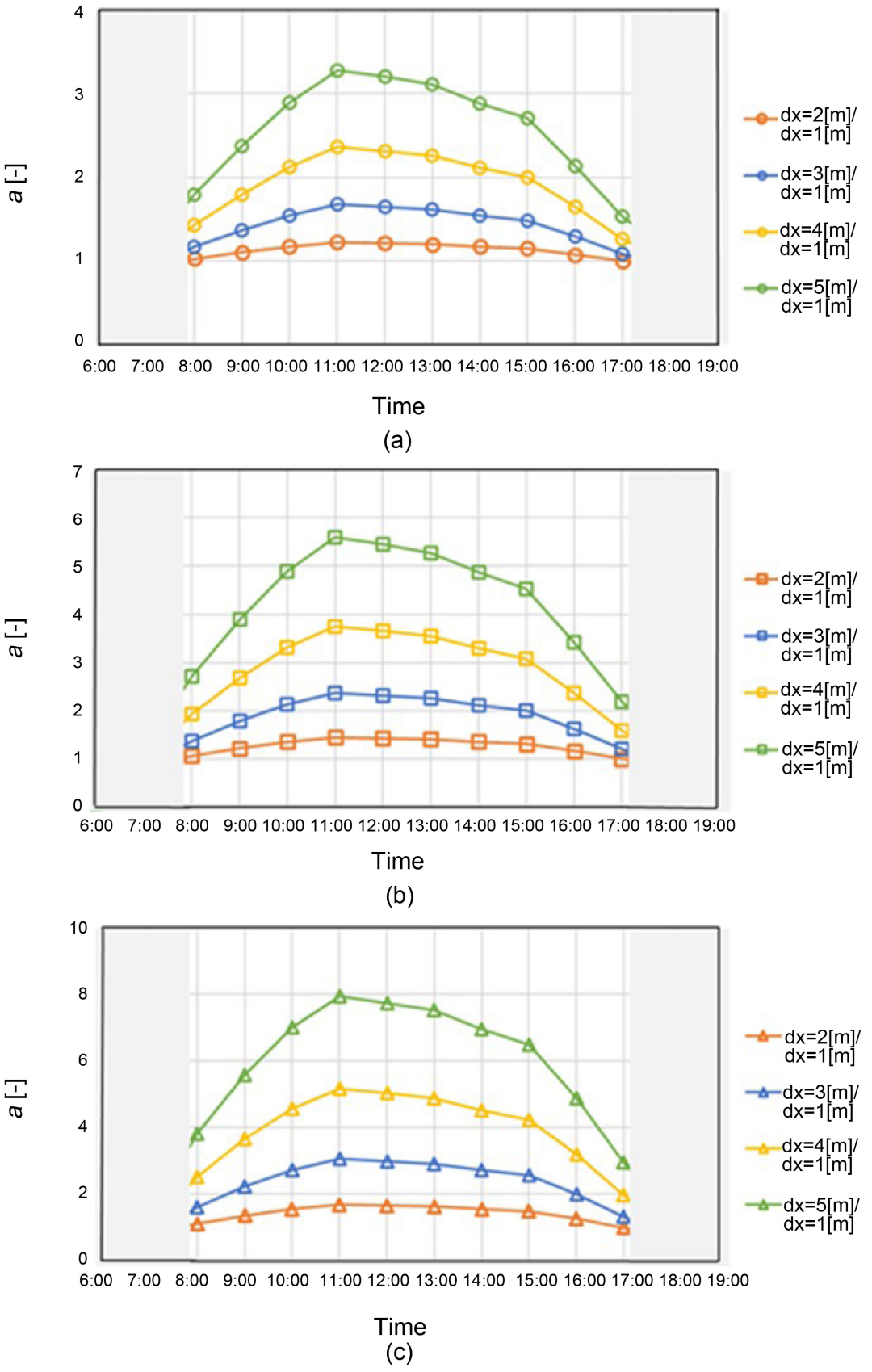

Figure 10. *a* with time changing *D* in July ((a): *D* = 0.5 [m], (b): *D* = 1.0 [m], (c): *D* = 1.5 [m]).

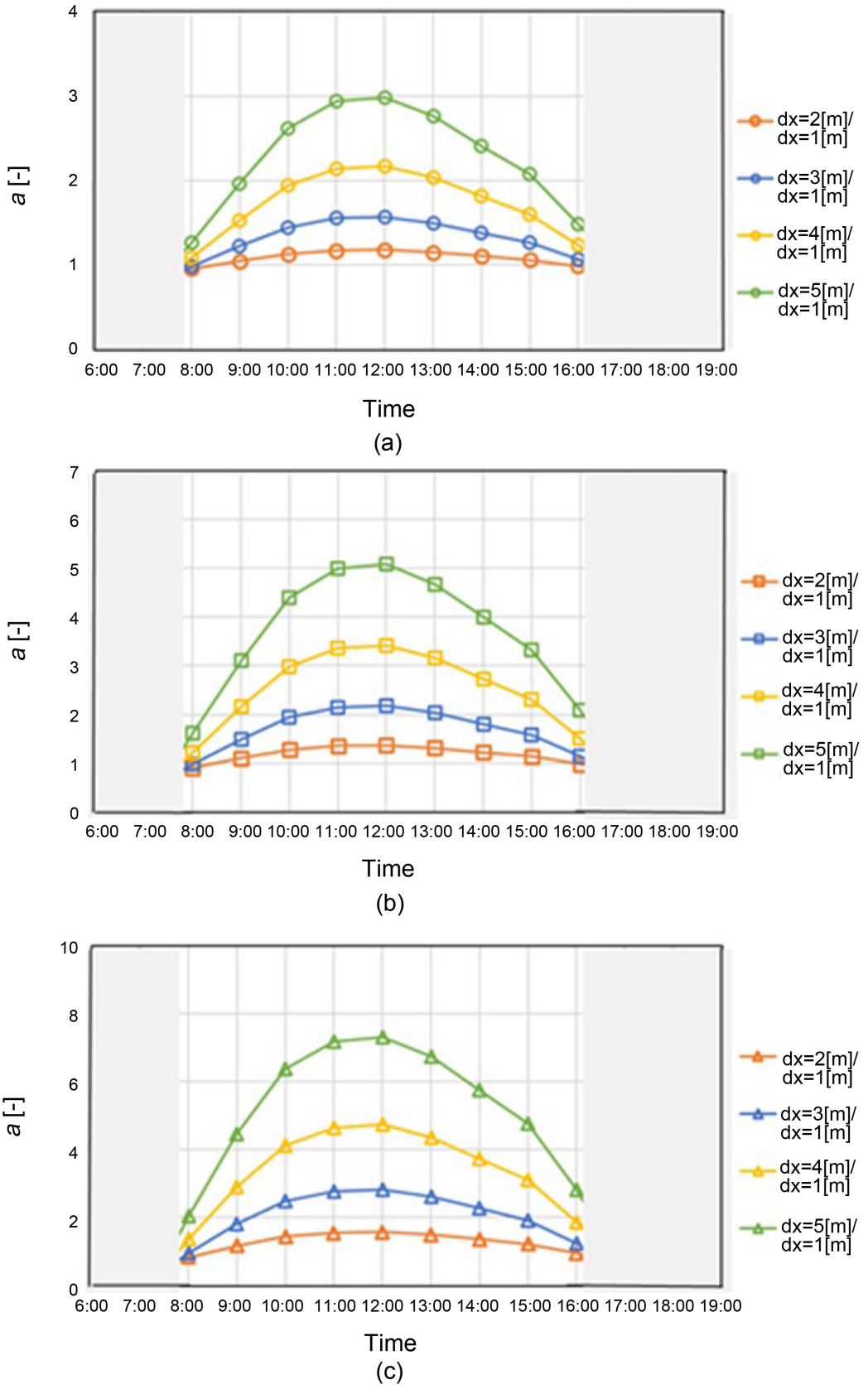

Figure 11. *a* with time changing *D* in October ((a): $D = 0.5$ [m], (b): $D = 1.0$ [m], (c): $D = 1.5$ [m]).

Table 6. The time when T_{fb} is over 873 K.

	7:00	8:00	9:00	10:00	11:00	12:00	13:00	14:00	15:00	16:00	17:00	18:00
Jan.					✓	✓	✓	✓				
Feb.				✓	✓	✓	✓	✓	✓			
Mar.			✓	✓	✓	✓	✓	✓	✓			
Apr.			✓	✓	✓	✓	✓	✓	✓	✓		
May			✓	✓	✓	✓	✓	✓	✓			
Jun.			✓	✓	✓	✓	✓	✓	✓	✓		
Jul.			✓	✓	✓	✓	✓	✓	✓	✓		
Aug.		✓	✓	✓	✓	✓	✓	✓	✓	✓	✓	
Sep.			✓	✓	✓	✓	✓	✓	✓			
Oct.			✓	✓	✓	✓	✓	✓	✓			
Nov.				✓	✓	✓	✓	✓				
Dec.					✓	✓	✓	✓				

marked in this table. When T_{fb} is over 873 K, this study assumes that H_2 can be produced.

The amount of H_2 produced from the biogas dry reforming reactor, when assuming to use the heat obtained from the solar collector for the conduction of biogas dry reforming, is calculated changing the conversion ratio of H_2 by 1%, 10% and 100%. Table 7 lists the amount of H_2 produced from the biogas dry reforming reactor.

According to Table 7, it is known that the amount of H_2 produced from the biogas dry reforming reactor is the highest in August, which is 74.55 kg in the case of conversion ratio of H_2 = 100%. The time when T_{fb} is over 873 K is the longest in August as shown in Table 6, resulting that the amount of H_2 produced from the biogas dry reforming reactor is the largest in August. In addition, it is seen from Table 7 that the amount of H_2 produced from the biogas dry reforming reactor is larger in June and July, while it is lower in January and December. Consequently, it can be claimed that it is prefer to produce H_2 in summer.

3.3. Estimation of the Power Generated by SOFC

This study assumes that the power is generated by SOFC over T_{fb} = 873 K changing the conversion ratio of H_2 by 1%, 10% and 100%. Table 8 lists the power generated by SOFC.

According to Table 8, it is known that the power generated by SOFC is the highest in August, which is 1380 kWh in the case of the conversion ratio of H_2 = 100%. The time when T_{fb} is over 873 K is the longest in August as shown in Table 6, resulting that the amount of H_2 produced from the biogas dry reforming reactor is the largest in August. In addition, it is seen from Table 8 that the power generated by SOFC is higher in June and July, while it is lower in January

Table 7. The amount of H_2 produced from the biogas dry reforming reactor under several conditions.

	Conversion ratio = 1%	Conversion ratio = 10%	Conversion ratio = 100%
January	0.2982 kg	2.982 kg	29.82 kg
February	0.4040 kg	4.040 kg	40.40 kg
March	0.5218 kg	5.218 kg	52.18 kg
April	0.5772 kg	5.772 kg	57.72 kg
May	0.5218 kg	5.218 kg	52.18 kg
June	0.5772 kg	5.772 kg	57.72 kg
July	0.5964 kg	5.964 kg	59.64 kg
August	0.7455 kg	7.455 kg	74.55 kg
September	0.5050 kg	5.050 kg	50.50 kg
October	0.5218 kg	5.218 kg	52.18 kg
November	0.3607 kg	3.607 kg	36.07 kg
December	0.2982 kg	2.982 kg	29.82 kg

Table 8. The power generated by SOFC under several conditions.

	Conversion ratio = 1%	Conversion ratio = 10%	Conversion ratio = 100%
January	5.51 [kWh]	55.1 [kWh]	551 [kWh]
February	7.46 [kWh]	74.6 [kWh]	746 [kWh]
March	9.64 [kWh]	96.4 [kWh]	964 [kWh]
April	10.7 [kWh]	107 [kWh]	1070 [kWh]
May	9.64 [kWh]	96.4 [kWh]	964 [kWh]
June	10.7 [kWh]	107 [kWh]	1070 [kWh]
July	11.0 [kWh]	110 [kWh]	1100 [kWh]
August	13.8 [kWh]	138 [kWh]	1380 [kWh]
September	9.33 [kWh]	93.3 [kWh]	933 [kWh]
October	9.64 [kWh]	96.4 [kWh]	964 [kWh]
November	6.66 [kWh]	66.6 [kWh]	666 [kWh]
December	5.51 [kWh]	55.1 [kWh]	551 [kWh]

and December. If the power generated by SOFC is supplied for the electricity demand of a couple household [16], 5.2 households can be supplied in August as the maximum, while 1.7 households can be supplied in January as the minimum. Consequently, it can be claimed that it is prefer to generate SOFC in summer, which follows the production of H_2 from the biogas dry reforming reactor.

According to the previous experimental studies by the authors [5] [6], the conversion ratio of H_2 is approximately 10%. Since the scale of biogas dry re-

forming reactor is a laboratory level, it is necessary to scale up the biogas dry reforming reactor or promote the thermal storage to prolong the time over T_{fb} = 873 K. Otherwise, the development of catalyst used for biogas dry reforming is needed. They are the future work in the experimental study.

4. Conclusion

This study has investigated the impact of climate data on the performance of solar collectors with various designs. In addition, this study has estimated the amount of H_2 produced from the biogas dry reforming reactor powered by the solar collectors. Moreover, this study has also estimated the power generated by SOFC with the produced H_2. It is revealed that T_{fb} and a are higher in spring and summer, resulting from the data of I. It can be claimed that dx = 4 m is the optimum length of solar absorber. The amount of H_2 produced from the biogas dry reforming reactor and the monthly power that could be generated by SOFC is the highest in August, which is 74.55 kg and 1380 kW respectively in the case of conversion ratio of H_2 = 100%. It is revealed that 5.2 households can be supplied by the power generated by SOFC in August as the maximum. It can be claimed that it is prefer to produce H_2 as well as to generate SOFC in summer.

Conflicts of Interest

The authors declare no conflicts of interest regarding the publication of this paper.

References

[1] Agency for Natural Resources and Energy (2012) Energy White Paper 2022. Agency for Natural Resources and Energy. https://www.meti.go.jp/english/report/pdf/0628_001b.pdf

[2] Jelle, B.P. (2016) Building Integrated Photovoltaics: A Concise Research Pathways. *Energies*, **9**, Article 21. https://doi.org/10.3390/en9010021

[3] World Bioenergy Association (2022) Global Bioenergy Statistics. World Bioenergy Association. https://www.worldbioenergy.org/uploads/211214%20WBA%20GBS%202021.pdf

[4] Mao, C., Chen, S., Shang, K., Liang, L. and Ouyang, J. (2022) Highly Active Ni-Ru Bimetallic Catalyst Integrated with MFI Zeolite-Loaded Cerium Zirconium Oxide for Dry Reforming of Methane. *ACS Applied Materials & Interfaces*, **14**, 47616-47632. https://doi.org/10.1021/acsami.2c12123

[5] Nishimura, A., Ohata, S., Okukura, K. and Hu, E. (2020) The Impact of Operating Conditions on the Performance of a CH_4 Dry Reforming Membrane Reactor for H_2 Production. *Journal of Energy and Power Technology*, **2**, Article No. 008. https://doi.org/10.21926/jept.2002008

[6] Nishimura, A., Takada, T., Ohata, S. and Kolhe, M.L. (2021) Biogas Dry Reforming for Hydrogen through Membrane Reactor Utilizing Negative Pressure. *Fuels*, **2**, 194-209. https://doi.org/10.3390/fuels2020012

[7] Bellos, E. and Tzivanidis, C. (2019) Alternative Designs of Parabolic trough Solar Collectors. *Progress in Energy and Combustion Science*, **71**, 81-117.

https://doi.org/10.1016/j.pecs.2018.11.001

[8] Osorio, J.D. and Rivera-Alvarez, A. (2022) Influence of the Concentration Ratio on the Thermal and Economic Performance of Parabolic trough Collectors. *Renewable Energy*, **181**, 786-802. https://doi.org/10.1016/j.renene.2021.09.040

[9] Bader, R., Pedretti, A., Barbato, M. and Steinfeld, A. (2015) An Air-Based Corrugated Cavity-Receiver for Solar Parabolic trough Concentrators. *Applied Energy*, **138**, 337-345. https://doi.org/10.1016/j.apenergy.2014.10.050

[10] Mohamad, A., Orfi, J. and Alansary, H. (2014) Heat Loss from Parabolic Trough Solar Collectors. *International Journal of Energy Research*, **38**, 20-28. https://doi.org/10.1002/er.3010

[11] Kumar, K.H., Daabo, A.M., Karmakar, M.K. and Hirani, H. (2022) Solar Parabolic Dish Collector for Concentrated Solar Thermal Systems: A Review and Recommendations. *Environmental Science and Pollution Research*, **29**, 32335-32367. https://doi.org/10.1007/s11356-022-18586-4

[12] Japan Meteorological Agency (2021) Past Meteorological Data Search. Japan Meteorological Agency. http://www.data.jma.go.jp/obd/stats/etrn/index.php

[13] Kreith, F. and Kreider, J.F. (1981) Preprints of Thermodynamics and Heat Transfer Applied to Solar Energy. In: *Solar Energy Handbook*, McGraw-Hill, New York.

[14] The Japan Society of Mechanical Engineers (1993) JSME Heat Transfer Handbook, Maruzen, Tokyo.

[15] NEDO (New Energy and Industry Technology Development Organization) (2023) Road Map 2017 of NEDO Fuel Cell and Hydrogen. NEDO. https://www.nedo.go.jp/content/100871973.pdf

[16] Power Design Com (2023) Daily Power Consumption of General Household. Power Design Com. https://standard-project.net/energy/statistics/energy-consumption-day.html